Control of Skyrmions in Confined Devices for Multistate Memory Application

Warda Al Saidi, Rachid Sbiaa, Suleiman Al Risi, Fatma Al Shanfari, Yannick Dusch, Nicolas Tiercelin

Control of skyrmions in confined devices for multistate memory application

W. Al Saidi[1], R. Sbiaa, [1,*] S. Al Risi[2], F. Al Shanfari[1], Y. Dusch[3], and N. Tiercelin[3]

[1]Sultan Qaboos University, Department of Physics, P.O. Box 36, PC 123, Muscat, Oman

[2]University of Technology and Applied Sciences, Engineering Department, Shinas, Oman

[3]University of Lille, CNRS, Centrale Lille, Université Polytechnique Hauts-de-France, UMR 8520 - IEMN, 59000 Lille, France

PACS 75.60.Ch– magnetic properties and materials

* Corresponding author: rachid@squ.edu.om

Abstract – The dynamics and stability of magnetic skyrmions within a nano-track with multiple confinements are investigated. The motion of a single skyrmion under a polarized electric current is studied. By adjusting the current magnitude and pulse width, the study reveals the possibility of pinning the skyrmion in each confinement. The depining of the skyrmion from the top confinement requires two pulses with adjustable time delay while a single pulse is enough to depin it for the case of bottom confinement. The study is extended to two skyrmions and it is found that once a skyrmion is pinned in one confinement, the second one stabilizes in the nearest available empty state. The results show that a multistate device could be obtained with the existence of only one skyrmion per state. This scheme offers an accurate way of controlling the resistance of the devices and thus could be used for multistate memory devices.

1. Introduction

A skyrmion is a magnetic quasiparticle with a swirling spin pattern that is topologically nontrivial. It is a two-dimensional object with a topology that can be described as a localized, smooth, and non-singular spin configuration. Since the first experimental observations of skyrmions in crystals [1,2] and thin ferromagnetic layers at room temperature [3,4], intensive studies have been focused on understanding their behavior. The nanoscale size and stability of these quasi-particle magnetic structures make them attractive for their implementation in different applications such as memory [5–8], logic [9] and neuromorphic computing [10–15]. Recently, it has been demonstrated that skyrmions can be created, displaced and annihilated by applying a magnetic field [16,17], spin transfer torque (STT) [18–21], spin-orbit torque [22], ultrafast heating pulses [23,24] or plasmonic resonance [25]. It is worth noting that skyrmions can be displaced with current density with values that could be better than 10^{11} A/m^2 [26] which is much lower than what is required for moving a magnetic domain wall case [27–29]. It has been reported that controlling the materials' intrinsic properties provides an easy way to tune the skyrmions' size and their velocity [30–33], which are among the key characteristics of a functional device; i.e. small size leads to higher memory capacity while high velocity reflects the speed of writing the data. Although the motion of skyrmions within nano-tracks has been widely investigated, their accurate positioning remains a challenge and has not been deeply investigated. In our previous work, we showed that creating stepped confinement could help pin and stabilize a skyrmion [33]. In this paper, we demonstrate the possibility of controlling the position of skyrmions in a multi-stepped nanowire. The study reveals that in the proposed design only a single skyrmion could be stabilized in each confinement. This is mainly due to the optimized confinement dimension. The flow of more than a skyrmion could be properly controlled along the nanowire. The effect of the repulsive force from the edge and the force between the skyrmions play a major role in the observed behavior.

2. Theoretical method

The theoretical model of multistate device generation is performed by micromagnetic simulation using Mumax3 software [34] which is based on solving the modified

Landau–Lifshitz–Gilbert (LLG) equation. For the case of current flowing in the plane of the film (CIP), the LLG equation can be written as

$$\frac{d\vec{m}}{dt} = -\gamma\, \vec{m} \times \vec{H}_e + \alpha\, (\vec{m} \times \frac{d\vec{m}}{dt}) + \vec{\Gamma}_{SST} \qquad (1)$$

The first and the second term on the right side of (1) are the precession and damping terms, respectively. The effective magnetic field $\vec{H}_e$ is expressed as:

$$\vec{H}_e = \frac{2A_e}{\mu_o M_S} \nabla^2 \vec{m} + \frac{2K_u}{\mu_o M_S} m_z \hat{z} + \vec{H}_D + \vec{H}_{DMI} \qquad (2)$$

The terms on the right side of (2) are the exchange field, the crystalline magnetic anisotropy field, the demagnetization field and the Dzyaloshinskii-Moriya interaction (DMI) field, respectively. The last term of Eq. (1) is associated with the STT effect in the case of a current flowing in the plane of the device and can be expressed by Zhang-Li form [35]

$$\vec{\Gamma}_{STT} = -(\vec{v}_s.\vec{\nabla})\vec{m} + \beta \vec{m} \times (\vec{v}_s.\vec{\nabla})\vec{m} \qquad (3)$$

where v_s is the effective spin-current drift velocity and β is the non-adiabatic spin torque parameter. The main objective of this study is to investigate a novel design for controlling the motion of the skyrmion in a memory device. We consider a 2 nm thick nano-track with a length of L = 780 nm and a width of 80 nm. Stepped regions with a size of 30 nm by 75 nm were added and removed from some parts of the track to localize the skyrmion position and to improve the linearity and repeatability of storage devices. The material intrinsic parameters used for this study are saturation magnetization M_S = 500 kA/m, exchange stiffness A_e = 15 pJ/m, Dzyaloshinskii Moriya interaction constant D = 3.3 mJ/m^2, Gilbert-damping coefficient α = 0.1 and the perpendicular magnetic anisotropy $K_u = 0.8 \times 10^6$ J/m^3. The shape anisotropy originated from the dipole-dipole interactions and caused a shift in the constant of uniaxial anisotropy in ultrathin film cases where the non-local effects are negligible [36,37]. The sample is discretized in small cells with the size of 2 × 2 × 2 nm^3. The values of M_s, K_u, A_{ex} and α are characteristics of (Co/Ni),

(Co/Pt) and (Co/Pd) multilayers [37–41]. They can be tuned in a wide range by adjusting the respective thicknesses and the number of repeats. The value of *D* in typical asymmetric structures where one Pt or Pd at the interface is substituted by Ir, W, and AlOx for instance [42–44]. The magnetic parameters used in this paper are similar to our previous work [33]. In the LLG equation, the calculation was carried out at 0 K to isolate and understand the intrinsic dynamics of skyrmions without thermal noise.

Firstly, a Néel-type skyrmion with topological charge Q = +1 is created near the left edge of the nano-track and then an electric current with a spin polarization efficiency P = 0.4 is injected into the nano-track in the CIP geometry to generate a motion of the skyrmion. The non-adiabatic torque coefficient β is fixed to 0.2 and the current flows toward the left so the electron would flow in the opposite direction. The device geometry is shown in Fig. 1(b-i).

3. Results and discussions

When the skyrmion is present in a wire it represents bit "1" while its absence at a particular position represents bit "0". To avoid information loss, the position of the skyrmion has to be fixed at a predefined position and the annihilation has to be avoided; hence in the present work, a constructed wire is used to create pinning regions for the skyrmion to define bit positions. Each region represents one bit, which corresponds to "0" if the region does not contain a skyrmion and "1" if the region contains one skyrmion.

3.1. Dynamics of a Single Skyrmion in Constricted Nanowire

In the first part of this study, the pinning and depinning of the skyrmion from the stepped regions under current pulses to create a multistate memory device is investigated. It can be seen from Fig. 1 that it is possible to achieve 8 states with 7 confined regions using a polarized current by displacing the skyrmion in the confinement regions. The calculations were carried out by creating a skyrmion on the left edge as the initial state and a sequence of current pulses were applied. Both the pulse width and the time delay between the pulses were fixed at 2 ns while the current density was varied. Fig. 1(a) shows the position *x* of the skyrmion along the nanowire versus time. In the inset of the graph, the magnitude of the current density and the

number of pulses are indicated. The first state was obtained for a pulse with magnitude $J = 6.0 \times 10^{11}$ A/m^2 indicated by number 1 in Fig. 1. It can be seen that the skyrmion moves with a constant velocity during the period of 2 ns when the current is applied as indicated by an almost straight line until it reaches a position of about 120 nm then bounces back and stabilizes. This small oscillation of the skyrmion seen before stabilized is due to the repulsive force from the edge. Skyrmion shows noticeable inertia-driven drift after the current pulse is removed rather than stopping immediately. The color scale in Fig. 1(b-i) represents the out-of-plane component m_z of the magnetization. The displacement of the skyrmion to state 2 (first top confined region) starting from the initial position can be realized by another single pulse with the same duration and $J = 3.0 \times 10^{11}$ A/m^2. The slightly attenuated oscillations after reaching the maximum position indicate that the skyrmion is swirling within the first confinement before stabilizing. All stated where achieved by starting from a fixed initial point, with state 1 being the initial reference point. Displacing the skyrmion from state 2 to state 3 requires two pulses; the first one to excite the skyrmion while the second one to move it to the third state. Here two pulses with the same magnitude of 5.5×10^{11} A/m^2 are applied. It is important to mention that the need for two pulses to move the skyrmion from the top confinements is due to the skyrmion Hall effect. It is known that the skyrmion Hall effect which is a deviation of the skyrmion path to the edge represents a challenge for skyrmion-based structures [45–48]. To overcome this issue, an antiferromagnetically coupled structure [49–52] and spin-orbit torque combined with STT [53] have been proposed to reduce skyrmion deviation to the edge effect. The other states could be obtained by altering the amplitude and number of pulses as indicated in Fig. 1(a). Interestingly, to pin the skyrmion in the upper confinement area (states 2, 4, 6 and 8), a single pulse is applied, whereas two pulses are required to move it to the lower confinement area (states 3, 5 and 7). Moreover, the pulse amplitude for the upper confinement was found to be fixed at 3.0×10^{11} A/m^2 while in the lower confinement, the amplitude changes depending on the history of the skyrmion. From Fig. 1, the oscillation in the x position with time is observed each time the skyrmion is driven from upper to lower states. In this part of the study, the time delay t_d between two consecutive pulses was fixed to 2 ns (Fig. 2). This parameter has to be adjusted to avoid the annihilation of the skyrmion as can be seen in Fig. 2(c) for $t_d = 1$ ns. In contrast, if the two pulses are largely delayed, as shown in Fig. 2(a) for $t_d = 3$ ns, the

skyrmion will not be displaced to the next state. As briefly discussed above, the first pulse is for exciting the skyrmion and making it ready for being displaced.

The effect of nanowire geometry on current-induced skyrmion dynamics was investigated. Fig. 2(d) is a plot of the skyrmion trajectory from state 1 to state 2, it is clear that the skyrmion is not moving in a straight line (blue line). The Magnus force acts in the direction normal to the drift velocity of the skyrmion and can therefore cause spiraling trajectories. The dashed lines indicate the border of the magnetic region. The sign of the skyrmion topological charge Q leads to the opposite direction of the topological Magnus force. It is found that the skyrmion rotation clockwise and counterclockwise depends on the sign of the skyrmion charge [54]. For the case of a Néel-type skyrmion with $Q = -1$, the motion is counterclockwise while for $Q = +1$ the direction of the skyrmion is clockwise. The radius of the path changes depending on the value of the Gilbert damping constant that affects the skyrmion Hall effect and the speed [55]. Here only one pulse is applied to move the skyrmion from state 1 to another stable state at the top confined region. Along its path, it was observed that the skyrmion size can be reduced due to the higher compression of the skyrmion by the barriers. It was observed that the size of the skyrmion was changing and reduced by about 1 nm at position 2 before expanding by about 2 nm when stabilized due to the dipolar repulsive force from the edge. The repulsive force from the edge causes the size of the skyrmion to decrease while passing through the states, if this force is too large in the case of a larger skyrmion or narrower channel for the skyrmion or larger current density, the skyrmion will annihilate. Both the intrinsic parameter and the geometry of the device need to be taken into account while designing the wire, more details can be found in Ref. 33. To move the skyrmion from state 2 to state 3 shown in Fig. 1, two pulses were used. The first one with $J = 5.5 \times 10^{11}$ A/m^2 and 2 ns pulse width for exciting the skyrmion and the second one with the same J and pulse width for displacing it to the next state. Fig. 3(a) is a plot of the skyrmion position along the nanowire x-direction to reach state 1 shown in Fig. 1. When the pulse current with $J = 6.0 \times 10^{11}$ A/m^2 is applied during the first 2 ns, there is a fast motion of the skyrmion represented by the left edge. For a larger current, the skyrmion can overcome the repulsive force from the first edge and be able to stabilize at the next state. Depending on the current density, the skyrmion can reach any one of the available stepped regions. Fig. 3(b) shows the velocity V_x of the skyrmion with time. A clear increase of V_x could be noticed until

reaching a maximum value of ~ 60 m/s before a sudden drop indicating a bouncing back of the skyrmion.

3.2. Two Skyrmions Dynamics in Constricted Nanowire

In the second part of this study, we considered the case of two skyrmions in a chain, initially located at the left side of the nanowire and the focus was on the possibilities of achieving higher numbers of states. We started with two skyrmions namely S_1 (leading) and S_2 (trailing) and we investigated their motion under a pulsed current similar to a single skyrmion case previously discussed. Initially, skyrmion S_1 is leading S_2 by about 50 nm. Under the same pulse with $J = 4.0 \times 10^{11}$ A/m^2 and a width of 2 ns, the leading skyrmion S_1 could be displaced to state 2 (top confinement) after overcoming the bottom barrier as shown in Fig. 4 (a). Inside the top confinement and because of the repulsive force as has been discussed in our previous work [33], S_2 undergoes a helical motion and stabilizes outside the confinement. The motion of trailing skyrmion S_2 is quite different. The color code represents the skyrmion radius, which is shrinking when it is closer to the bottom or top edges. The trailing skyrmion S_2 could not reach the top confinement due to the strong interaction with S_1. It can be seen from Fig. 4(a) that S_2 was back due to the existence of S_1. The dimension of the confinement and the repulsive interaction skyrmion-skyrmion allows the stability of only one skyrmion per state. Firstly, the size of S_1 is reduced close to the bottom step and when it is closer to S_2 before bouncing back. The snapshots in Figs. 4(b-d) show the positions and size of S_1 and S_2 in three different situation. In Fig. 4(b), S_1 which is very close to the edge of the bottom stepped region, shrinks in size are reported in Fig. 5(b) and indicated by the state A. The radius of S_2 remains unchanged. A second reduction of S_1 radius occurs at state B in Fig. 5(b) corresponding to when it reaches the right edge of the top confinement. This state can also be seen in the snapshot of Fig. 4(c). The third reduction of S_1 happens when it is closer to S_2 corresponding to state C in Fig. 5(b) and snapshot of Fig. 4(d). On the other hand, the size of S_2 is reduced continuously when it is approaching the stepped region until reaches its minimum (~ 20 nm) when it is also close to S_1 as shown in Fig. 4(a). Fig. 5(a) is a plot of the position of the two skyrmions and the separation between them as a function of time. The positions r_1 and r_2 are taken from the left-bottom edge of the nanowire and the dashed regions in Fig. 5 indicate the

stepped region. The skyrmion-skyrmion repulsive force is maximal when S_1 and S_2 are very close (minimum S) which corresponds to a small radius for both skyrmions.

For $J = 5.0 \times 10^{11}$ A/m^2 of 4 ns duration, it can be seen from Fig. 6(a) that both S_1 and S_2 overcome the first non-magnetic barrier (bottom stepped area) but S_1 could reach the next bottom confinement while S_2 was again bounced back to the top confinement. For S_2, this is the only nearest available state. By following the path of both skyrmions, one can see from Fig. 6(b) that there is a repulsive force between S_1 and S_2, which is responsible for the deviation of S_2 from reaching the same state as S_1. The dashed region in Fig. 6(a) represents the magnetic part of the device. From two interacting skyrmions, it could be seen that under the device geometry, only one skyrmion could be stabilized in each confined region.

4. Conclusion

Towards a multistate spintronics device, a stepped nano-track with bottom and top confinements was proposed. For a common material with perpendicular magnetic anisotropy, the adjustment of current magnitude and its duration enables the displacement of the skyrmion at any position. Furthermore, the study of two skyrmions shows the possibility of moving them accurately with only one skyrmion in each confinement. The dimension of the confinement and the repulsive forces from the edge and from skyrmion-skyrmion are responsible for this finding. Due to the Hall angle, depinning a skyrmion from bottom confinement needs only a single pulse current with an optimal magnitude and duration while two pulses are necessary for depinning from top confinement. If the time delay t_d between the two pulses is too short, the skyrmion collapses and if t_d is too large, the skyrmion remains pinned. The dynamic of a large number of skyrmions created at one side shows the possibility of stabilizing/pinning a single skyrmion in each confinement. These results open the way for large-capacity memory devices and neuromorphic computing.

Acknowledgments

R. Sbiaa would like to acknowledge the support from the HMTF Strategic Research of Oman (grant no. SR/SCI/PHYS/20/01).

References

[1] S. Mühlbauer *et al.*, Skyrmion Lattice in a Chiral Magnet, Science **323** 915 2009.

[2] X. Z. Yu *et al.*, Real-space observation of a two-dimensional skyrmion crystal, Nature **465** 901 2010.

[3] C. Moreau-Luchaire *et al.*, Additive interfacial chiral interaction in multilayers for stabilization of small individual skyrmions at room temperature, Nat. Nanotechnol. **11** 444 (2016).

[4] S. Woo *et al.*, Observation of room-temperature magnetic skyrmions and their current-driven dynamics in ultrathin metallic ferromagnets, Nat. Mater. **15** 501(2016).

[5] R. Tomasello, E. Martinez, R. Zivieri, L. Torres, M. Carpentieri and G. Finocchio, A strategy for the design of skyrmion racetrack memories, Sci. Rep. **4** 6784 (2014).

[6] A. Fert, V. Cros and J. Sampaio, Skyrmions on the track, Nat. Nanotechnol. **8** 152 (2013).

[7] L. Wang *et al*., Construction of a Room-Temperature Pt/Co/Ta Multilayer Film with Ultrahigh-Density Skyrmions for Memory Application, ACS Appl. Mater. Interfaces **11** 12098 (2019).

[8] M. G. Morshed, H. Vakili, and A. W. Ghosh, Positional Stability of Skyrmions in a Racetrack Memory with Notched Geometry, Phys. Rev. Appl. **17** 064019 (2022).

[9] S. Luo and L. You, Skyrmion devices for memory and logic applications, APL Mater. **9** 050901 (2021).

[10] S. Li, W. Kang, Y. Huang, X. Zhang, Y. Zhou and W. Zhao, Magnetic skyrmion-based artificial neuron device, Nanotechnology **28** 31LT01 (2017).

[11] D. Prychynenko *et al.*, Magnetic Skyrmion as a Nonlinear Resistive Element: A Potential Building Block for Reservoir Computing, Phys. Rev. Appl. **9** 014034 (2018).

[12] K. M. Song *et al.*, Skyrmion-based artificial synapses for neuromorphic computing, Nat. Electron. **3** 148 (2020).

[13] J. Grollier, D. Querlioz, K. Y. Camsari, K. Everschor-Sitte, S. Fukami and M. D. Stiles, Neuromorphic spintronics, Nat. Electron. **3** 360 (2020).

[14] R. Klaus, *et al.*, Brownian reservoir computing realized using geometrically confined skyrmion dynamics. Nature Commu. **13** 6982 (2022).

[15] Z. Zhizhong *et al.*, Magnon scattering modulated by omnidirectional hopfion motion in antiferromagnets for meta-learning, Science Adv. **9** (2023), DOI: 10.1126/sciadv.ade7439.

[16] N. Romming et al., Writing and Deleting Single Magnetic Skyrmions, Science **341** 636 (2013).

[17] A. Casiraghi *et al.*, Individual skyrmion manipulation by local magnetic field gradients, Comm. Phys. **2** 145 (2019).

[18] J. Sampaio, V. Cros, S. Rohart, A. Thiaville and A. Fert, Nucleation, stability and current-induced motion of isolated magnetic skyrmions in nanostructures, Nat. Nanotechnol. **11** 839 (2013).

[19] W. Legrand *et al.*, Room-Temperature Current-Induced Generation and Motion of sub-100 nm Skyrmions, Nano Lett. **17** 2703 (2017).

[20] W. Wang *et al.*, Electrical manipulation of skyrmions in a chiral magnet, Nat. Commun. **13** 1593, (2022).

[21] R. Juge *et al.*, Skyrmions in synthetic antiferromagnets and their nucleation via electrical current and ultra-fast laser illumination, Nat. Commun. **13** 4807 (2022).

[22] F. Büttner *et al.*, Field-free deterministic ultrafast creation of magnetic skyrmions by spin-orbit torques, Nat. Nanotechnol. **12** 1040 (2017).

[23] N. Novakovic-marinkovic *et al.*, From stripes to bubbles : Deterministic transformation of magnetic domain patterns in Co / Pt multilayers induced by laser helicity, Phys. Rev. **B102** 174412 (2020).

[24] F. Büttner *et al.*, Thermal nucleation and high-resolution imaging of submicrometer magnetic bubbles in thin thulium iron garnet films with perpendicular anisotropy, Phys. Rev. Mater. **4** 011401 (2020).

[25] W. Al Saidi, Y. Dusch, N. Tiercelin, and R. Sbiaa, Ultrafast skyrmion generation by plasmonic resonance, Phys. rev B **15** 184427 (2024).

[26] L. Peng, K. Karube, Y. Taguchi, N. Nagaosa, Y. Tokura and X. Yu, "Dynamic transition of current-driven single-skyrmion motion in a room-temperature chiral-lattice magnet," Nat. Commun. **12** 6797 (2021).

[27] H. Tanigawa, T. Suzuki, S. Fukami, K. Suemitsu, N. Ohshima and E. Kariyada, Thickness dependence of current-induced domain wall motion in a Co/Ni multi-layer with out-of-plane anisotropy, Appl. Phys. Lett. **102** 152410 (2013).

[28] R. Sbiaa and S. N. Piramanayagam, Multi-level domain wall memory in constricted magnetic nanowires, Appl. Phys. A Mater. Sci. Process. **114** 1347 (2014).

[29] H. Mohammed, S. A. Risi, T. L. Jin, J. Kosel, S. N. Piramanayagam and R. Sbiaa, Controlled spin-torque driven domain wall motion using staggered magnetic wires, Appl. Phys. Lett. **116** 032402 (2020).

[30] X. S. Wang, H. Y. Yuan, and X. R. Wang, A theory on skyrmion size, Comp. Phys. **1** 31 (2018).

[31] M. Fattouhi, M. Y. El Hafidi and M. El Hafidi, Skyrmion size evolution with interlayer exchange coupled ferromagnetic nanostructures, Phys. Lett. A **384** 126260 (2020).

[32] A. K. Behera, S. S. Mishra, S. Mallick, B. B. Singh and S. Bedanta, Size and shape of skyrmions for variable Dzyaloshinskii–Moriya interaction and uniaxial anisotropy, J. Phys. D. Appl. Phys. **51** 285001 (2018).

[33] W. Al Saidi and R. Sbiaa, Stabilizing magnetic skyrmions in constricted nanowires, Sci. Rep. **12** 10141 (2022).

[34] A. Vansteenkiste, J. Leliaert, M. Dvornik, M. Helsen, F. Garcia-Sanchez and B. Van Waeyenberge, The design and verification of MuMax3, AIP Adv. **4** 07133 (2014).

[35] S. Zhang and Z. Li, Roles of Nonequilibrium Conduction Electrons on the Magnetization Dynamics of Ferromagnets, Phys. Rev. Lett. **93** 127204 (2004).

[36] F. Garcia, F. Fettar, S. Auffret, B. Rodmacq and B. Dieny, Exchange-biased spin valves with perpendicular magnetic anisotropy based on (Co/Pt) multilayers, J. Appl. Phys. **93** 8397 (2003).

[37] K. Yakushiji *et al.*, Ultrathin Co/Pt and Co/Pd superlattice films for MgO-based perpendicular magnetic tunnel junctions, Appl. Phys. Lett. **97** 232508 (2010).

[38] S. Pal, B. Rana, O. Hellwig, T. Thomson and A. Barman, Tunable magnonic frequency and damping in [Co/Pd]8 multilayers with variable Co layer thickness, Appl. Phys. Lett. **98** 082501 (2011).

[39] R. Sbiaa, J. M. Shaw, H. T. Nembach, M. Al Bahri, M. Ranjbar, J. Åkerman, and S. N. Piramanayagam, Ferromagnetic resonance measurements of (Co/Ni/Co/Pt) multilayers with perpendicular magnetic anisotropy, J. Phys. D: Appl. Phys. **49** 425002 (2016).

[40] T. Kalaycı, C. Deger, S. Akbulut and F. Yildiz, Tuning magnetic properties of non-collinear magnetization configuration in Pt/$[Pt/Co]_6$/Pt/Co/Pt multilayer structure, J. Magn. Magn. Mater. **436** 11 (2017).

[41] A. Al Subhi and R. Sbiaa, Control of magnetization reversal and domain structure in (Co/Ni) multilayers, J. Magn. Magn. Mater. **489** 165460 (2019).

[42] M. Belmeguenai *et al.*, Interfacial Dzyaloshinskii-Moriya interaction in perpendicularly magnetized Pt/Co/AlOx ultrathin films measured by Brillouin light spectroscopy, Phys. Rev. **B91** 180405 (2015).

[43] M. Baćani, M. A. Marioni, J. Schwenk, and H. J. Hug, How to measure the local Dzyaloshinskii-Moriya Interaction in Skyrmion Thin-Film Multilayers, Sci. Rep. **9** 1 (2019).

[44] S. K. Jena *et al.*, Interfacial Dzyaloshinskii–Moriya interaction in the epitaxial W/Co/Pt multilayers, Nanoscale **13** 7685 (2021).

[45] J. Iwasaki, W. Koshibae, and N. Nagaosa, Colossal Spin Transfer Torque Effect on Skyrmion along the Edge, Nano Lett. **14** 4432 (2014).

[46] K. Litzius *et al.*, Skyrmion Hall effect revealed by direct time-resolved X-ray microscopy, Nat. Phys. **13** 170 (2017).

[47] G. Chen, Skyrmion Hall effect, Nat. Phys. **13** 112 (2017).

[48] R. Juge *et al.*, Current-Driven Skyrmion Dynamics and Drive-Dependent Skyrmion Hall Effect in an Ultrathin Film, Phys. Rev. Appl. **12** 044007 (2019).

[49] X. Zhang, Y. Zhou and M. Ezawa, Magnetic bilayer-skyrmions without skyrmion Hall effect, Nat. Commun. **7** 10293 (2016).

[50] M. W. Daniels, W. Yu, R. Cheng, J. Xiao and D. Xiao, Topological spin Hall effects and tunable skyrmion Hall effects in uniaxial antiferromagnetic insulators, Phys. Rev. **B99** 224433 (2019).

[51] J. Barker and O. A. Tretiakov, Static and Dynamical Properties of Antiferromagnetic Skyrmions in the Presence of Applied Current and Temperature, Phys. Rev. Lett. **116** 147203 (2016).

[52] C. Jin, C. Song, J. Wang and Q. Liu, Dynamics of antiferromagnetic skyrmion driven by the spin Hall effect, Appl. Phys. Lett. **109** 182404 (2016).

[53] J. Plettenberg, M. Stier and M. Thorwart, Steering of the Skyrmion Hall Angle by Gate Voltages, Phys. Rev. **B124** 207202 (2020).

[54] M. Weißenhofer and U. Nowak, Topology dependence of skyrmion Seebeck and skyrmion Nernst effect, Sci. Rep. 12 6801 (2022).

[55] Y. Ishida and K. Kondo, An effect of the Gilbert damping constant on the skyrmion Hall effect, J. Magn. Magn. Mater. **493** 165687 (2020).

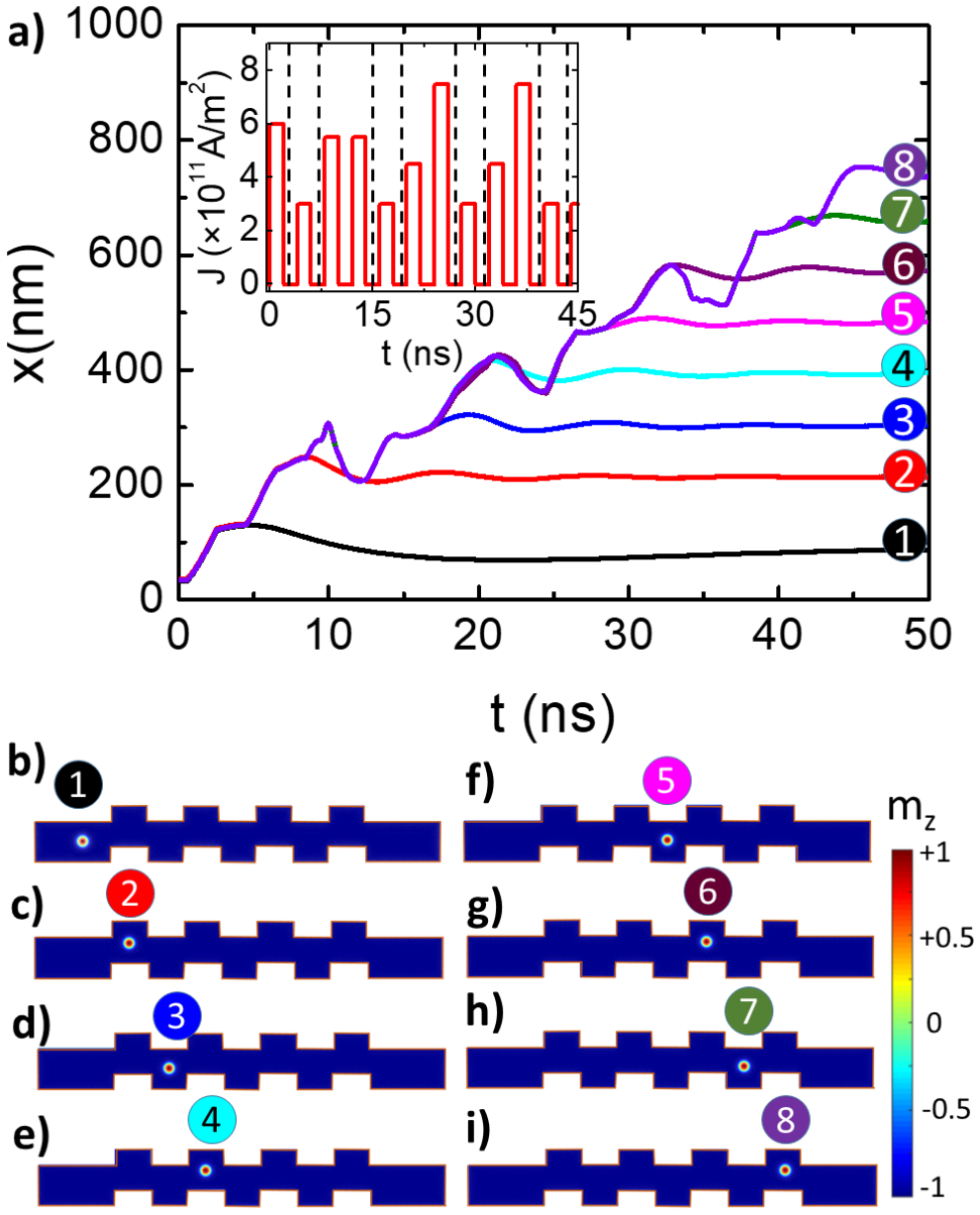

Fig. 1. (a) Time dependence of the skyrmion position for different current density values. After each pulse, the time dependence of the position *x* is recorded. The following pulse is applied by considering the skyrmion at the initial state. Inset is the current density magnitude versus time. To reach states 3, 5 and 7, two pulses were necessary. The inset is an enlarged *x* position of the skyrmion showing that the skyrmion stabilized at the top confined region and swirled in that region before moving to the next bottom confinement. (b)-(i) snapshots of magnetic states as in (a). The length of the wire is L = 780 nm, the width w = 80 nm and the thickness is 2 nm. The color scale shows the out-of-plane component of magnetization.

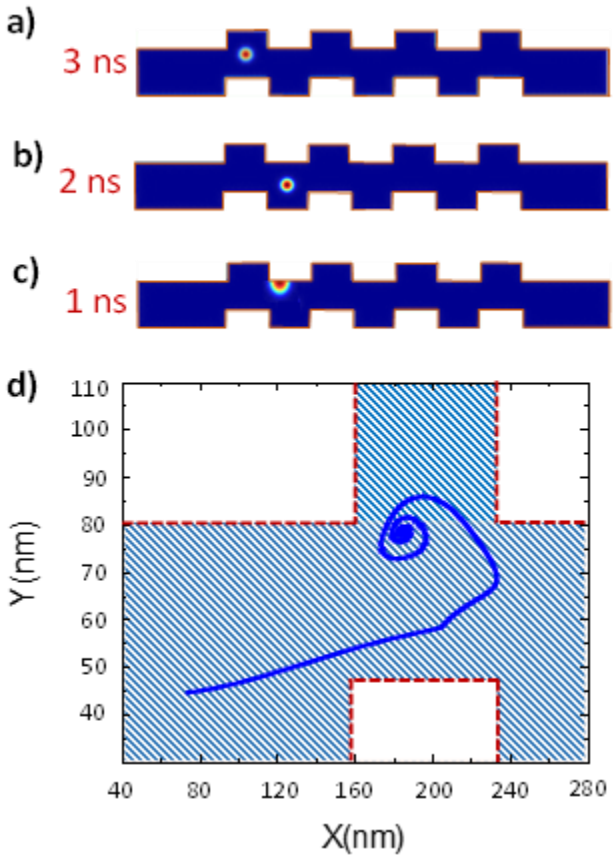

Fig. 2. (a) The skyrmion remains pinned when the time delay is larger than 2.8 ns, (b) the skyrmion moves to the third state when the time delay is between 1 and 2.7 ns and (c) annihilation of the skyrmion when the time delay is less than 1 ns for two fixed pulses of 5.5×10^{11} A/m^2 and 2 ns duration. (d) The skyrmion trajectory from state 1 to state 2 shows counter-clockwise spiral motion under a pulsed current of 3.0×10^{11} A/m^2 for 2 ns duration.

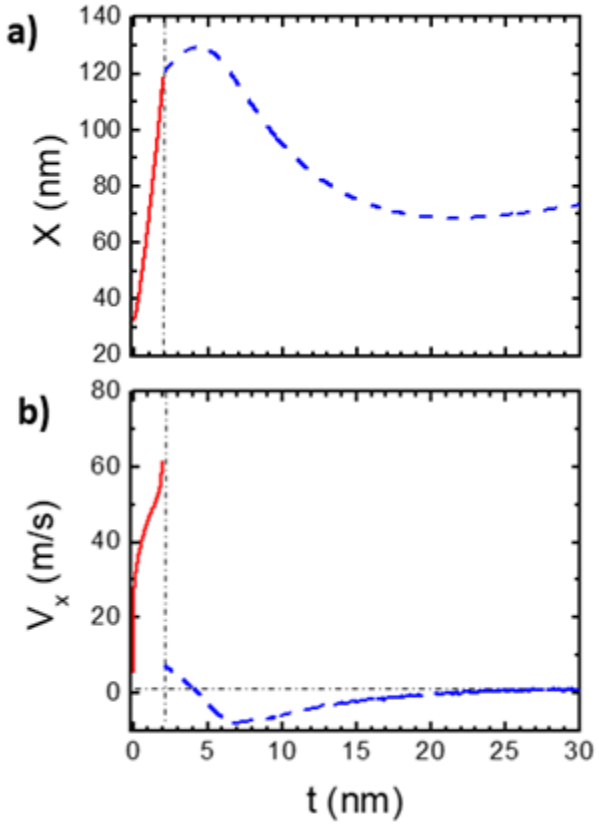

Fig. 3. (a) The *x*-position and (b) the velocity of the skyrmion versus time when a current density of 3.0 × 10^{11} A/m^2 is applied for 2 ns. The solid and dashed lines are when the current is on and off, respectively.

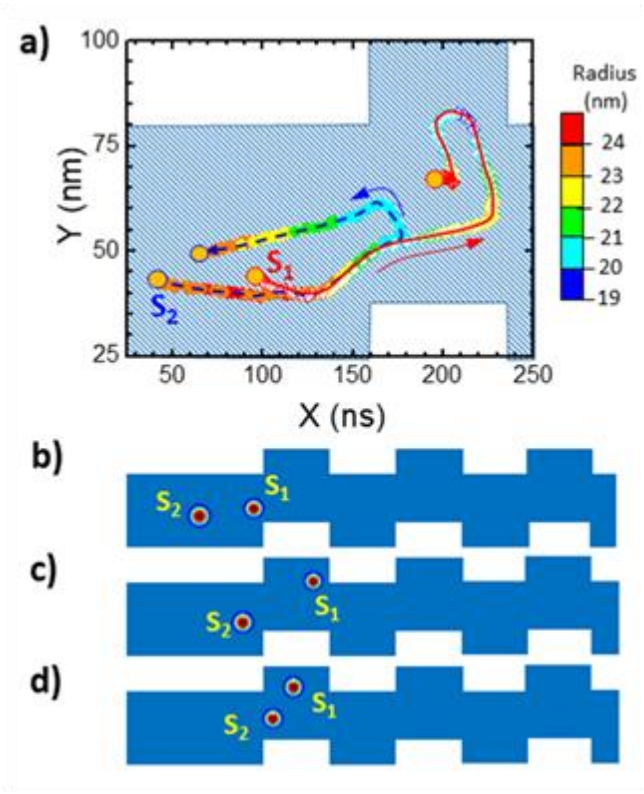

Fig. 4. (a) The Path of skyrmion S_1 (solid line) and skyrmion S_2 (dotted line) under a current density of 4×10^{11} A/m^2 for 2 ns duration. The code bar represents the radius of S_1 and S2. The trailing skyrmion S_2 was bounced back due to the interaction with the leading one S_1. This later was stabilized near the confined region but not inside because of the net edges repulsive force. (b) to (d) are snapshots of skyrmions S_1 and S_2 within the device at different positions. These images are taken at the three states A, B and C indicated in Fig. 5(b).

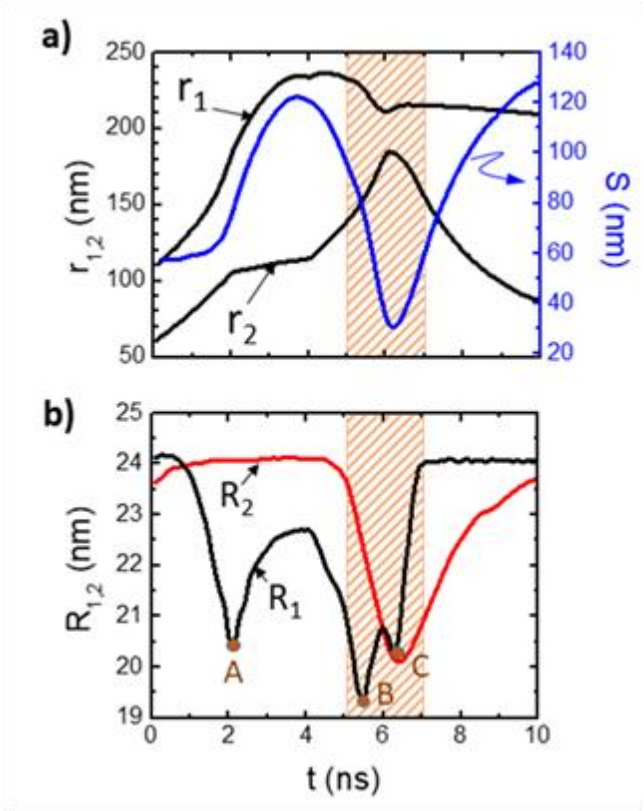

Fig. 5. (a) The time dependence of the positions of S_1 and S_2 and the separation between. (b) The radius of S_1 and S_2 as a function of the time. The dashed regions indicate the stepped region.

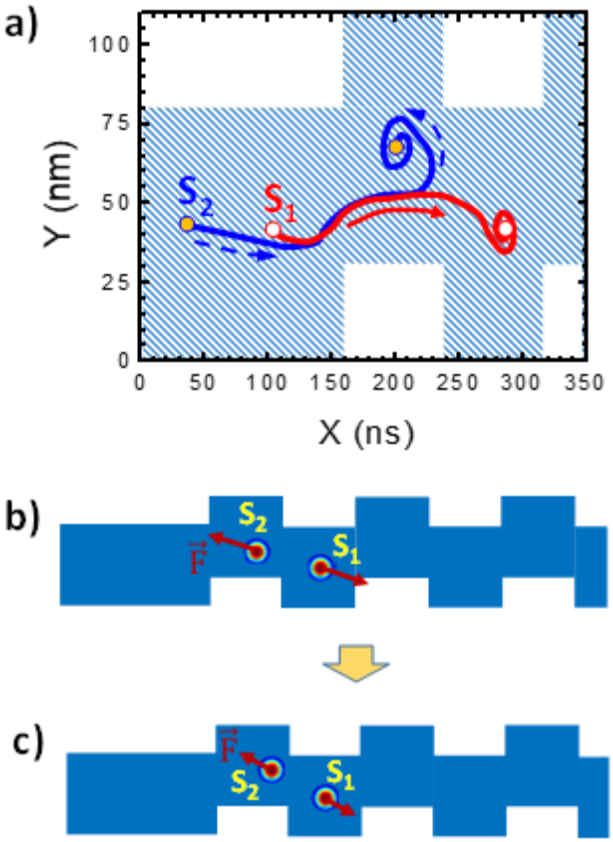

Fig. 6. (a) The Path of skyrmion S_1 (solid line) and skyrmion S_2 (dotted line) under a current density of 5×10^{11} A/m^2 for 4 ns duration. The trailing skyrmion S_2 was bounced back to the top confinement due to the interaction with leading one S_1. This later was stabilized near the bottom confined region but not inside because of the net edges repulsive force. (b) and (c) are snapshots of skyrmions S_1 and S_2 within the device at different positions. The arrows represent the repulsive forces between S_1 and S_2.